THE ASTROPHYSICAL JOURNAL, 312:183–194, 1987 January 1

COSMIC-RAY POSITRONS FROM 10 TO 20 GeV: A BALLOON-BORNE MEASUREMENT USING THE GEOMAGNETIC EAST-WEST ASYMMETRY[1]

DIETRICH MÜLLER[2] AND KWOK-KWONG TANG
Enrico Fermi Institute, University of Chicago
Received 1986 May 2; accepted 1986 June 27

ABSTRACT

We report results on cosmic-ray positrons obtained in a balloon flight of the University of Chicago electron telescope in Hawaii in 1984 April. Making use of the east-west asymmetry in the geomagnetic cutoff rigidity, we have successfully separated cosmic-ray positrons and negatrons over the range 10–20 GeV. The resulting positron to electron ratio, $e^+/(e^+ + e^-)$, is 17% ± 5%, significantly higher than the ratio measured in the 1–10 GeV range by other experiments. This increase appears to suggest that either a primary component of positrons becomes significant above 10 GeV or that the spectrum of primary negatrons decreases above 10 GeV more sharply than that of secondary positrons.

Subject headings: cosmic rays: abundances — elementary particles

I. INTRODUCTION

High-energy electrons in the cosmic particle radiation interact with the electromagnetic components of the interstellar medium by synchrotron radiation or inverse Compton scattering. Energy losses due to these interactions strongly affect the propagation and lifetime of electrons in interstellar space and are reflected in the shape of the observed energy spectrum. Measurements of cosmic-ray electrons therefore reveal aspects of the source distribution and galactic propagation of cosmic rays that are not observable in the nuclear cosmic radiation, and may also provide insight into the electromagnetic conditions in interstellar space.

Electrons consist of positrons and negatrons. Individual observations of the two oppositely charged species are much more difficult to perform than measurements of the overall flux and energy spectrum. Therefore, experimental data on the relative abundance of positrons and negatrons become very scarce above 10 GeV, while information on the overall energy spectrum of electrons exists up to energies in excess of 1000 GeV. A striking feature of the observed energy spectrum is its steep spectral slope. Figure 1 shows the results of the University of Chicago group, compared with recent data of Golden *et al.* (1984) and with the high-energy data of Nishimura *et al.* (1981). We note that several earlier measurements, mostly below 100 GeV, give electron fluxes differing by as much as a factor of 2 from those shown in Figure 1. However, most observers agree that the electron spectrum beyond 10 GeV drops much faster than that of any nuclear cosmic-ray species, and that the differential flux above 100 GeV can be fitted with a power law $E^{-\Gamma}$, with $\Gamma = 3.4 \pm 0.2$. This spectral steepening is commonly assumed to be the consequence of radiative energy losses (whose rate increases proportional to E^2) that dominate at high energies over the physical loss of electrons by escape from the Galaxy. Using the "leaky box" approximation of cosmic-ray propagation in the Galaxy, and assuming a source spectrum with a single power-law slope close to that of the locally observed spectrum of protons, one derives from the observed steepening a value of the galactic containment time of $\sim 10^7$ yr (Prince 1976; Tang 1984). This value is in remarkable agreement with the containment time determined on the basis of measurements of the radioactive "clock" isotope Be^{10} at much lower energies (Garcia-Munoz, Mason, and Simpson 1977, Wiedenbeck and Greiner 1980). However, this agreement might be accidental: measurements of the elemental composition of cosmic-ray nuclei, specifically of the relative abundances of spallation-produced secondary nuclei (e.g., Juliusson, Meyer, and Müller 1972), lead one to expect a decrease of the containment time with increasing energy. To resolve this issue, one needs independent information on the origin of cosmic-ray electrons and on their energy spectrum at the source (i.e., before it is deformed as a result of loss processes during propagation).

Electrons can be produced as secondary particles (mainly via the π-μ-e decay) subsequent to interactions of nuclear cosmic rays in the interstellar gas. This process leads to about equal fractions of negatrons and positrons. The production spectra can be calculated for various propagation models (e.g., Orth and Buffington 1976) and are directly related to the energy spectrum of parent protons. In the limited energy region where the separation of positrons and electrons has been possible (mostly below 10 GeV), a large negatron enhancement is observed (Fanselow *et al.* 1969; Beuerman *et al.* 1970; Daugherty, Hartman, and Schmidt 1975). This negatron flux must originate in primary acceleration sites. Consequently, one commonly assumes that the majority of electrons are primary particles, even at high energies where the negatron to positron abundance ratio is unknown. At the same time, positrons are generally taken as almost entirely of secondary origin. To test these assumptions, and thus to obtain solid information on the origin of electrons, separate measurements of positrons and negatrons over a larger energy region are needed. At the same time, such measurements will lead to a much improved understanding of the effects of radiative energy losses during propagation.

The measurement of positrons is a very difficult task because their small flux necessitates large detectors, and because of the need of powerful discrimination against the much larger (by a factor 10^3–10^4) flux of protons. This task has been accomplished with balloon-borne magnet spectrometers. Below 10 GeV, permanent magnets could be used (e.g., Fanselow

[1] Work supported, in part, by NASA grant NSG 7464.
[2] Also Department of Physics, University of Chicago.

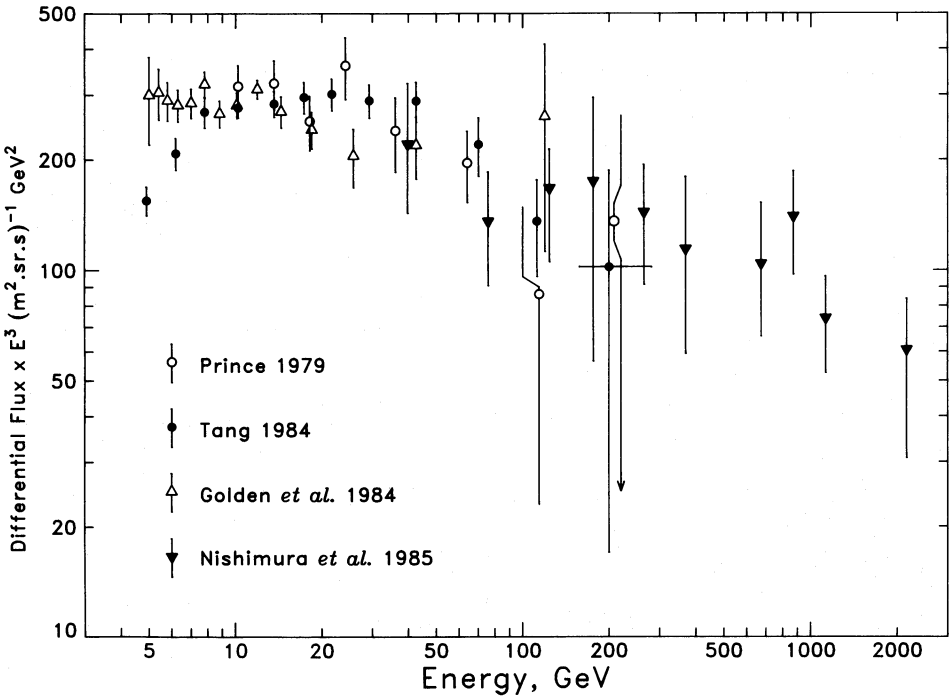

FIG. 1.—Differential energy spectrum of electrons multiplied by E^3. Figure includes only the most recent results, published since 1979. Data of Golden *et al.* are negatron fluxes multiplied by 1.1 and transformed to the interstellar medium. The other experiments were measurements of the total electron flux at the top of the atmosphere.

et al. 1969), while somewhat higher energies were reached with superconducting magnets (Buffington, Orth, and Smoot 1975; Golden *et al.* 1985). Nevertheless, the available data are quite scarce and uncertain beyond 10 GeV.

An alternate opportunity to separate positive and negative particles is provided by the Earth's magnetic field. The cutoff rigidity at a given geographic location varies with the direction of incidence of the particle, and with the particle's polarity. For instance, Figure 2 shows how the cutoff rigidities vary with the direction of incidence for negatrons at Hawaii. The cutoff structure for positrons is similar, except that east and west exchange roles. Thus, for certain directions and rigidity ranges, the Earth's magnetic field may transmit only particles of one polarity but not the other. The utilization of this effect to separate electrons and positrons was pioneered by Daniel and Stephens (1965, 1967). However, the first measurements (Anand, Daniel, and Stephens 1969; Agrinier *et al.* 1969) were severely limited because of insufficient statistics and systematic uncertainties.

In principle, the geomagnetic field should permit measurements of positrons and electrons up to energies around 35 GeV. In order to make such a measurement a success one needs a detector that exhibits (*a*) a large area for good counting statistics, (*b*) good energy resolution for individual electrons, (*c*) capability of recording the trajectory of each particle, and (*d*) high discrimination power ($\sim 10^4$) against protons. In addition, the measurement must be able to correct for background of directly produced atmospheric secondaries or of reentrant albedo particles. We believe that our balloon-borne electron telescope, which had been flown successfully in previous years to measure the overall flux and energy spectrum of electrons (Hartmann, Müller, and Prince 1977; Prince 1979; Tang 1984), does fulfill these experimental requirements. We have therefore used this instrument, with some modifications, in a balloon flight from Hawaii (vertical geomagnetic cutoff rigidity 12.8 GV) in 1984 April, and we have been successful in determining the positron fraction in the galactic cosmic rays over the range 10–20 GeV. In the following, we shall describe and discuss this investigation.

II. INSTRUMENTATION

A cross section of the detector is shown in Figure 3. Since the design principles of this instrument have been described previously (Prince 1979; Tang 1984), we shall just briefly summarize the main features. The instrument is an electronic counter telescope with geometric factor of 0.1 m^2 sr, consisting of a large plastic scintillator T1, a transition radiation detector (TRD) of six radiator-detector pairs, and a lead-scintillator shower detector (S) of 18.5 radiation length depth. During the balloon flight, the instrument is triggered by particles which register in T1 and show interactions in S above a threshold equivalent to a 3 GeV electron shower.

For each event, the following measurements are made: (*a*) the magnitude of the charge Z is measured with T1; (*b*) the direction of traversal is determined by a time-of-flight measurement between T1 and S; (*c*) the trajectory through the instrument is obtained with a hodoscope formed by the multiwire proportional chambers of the TRD; (*d*) six measurements of the ionization and transition radiation signals along the trajectory are made in the TRD; and (*e*) the pulse heights in the shower counter S are recorded to measure the electron energy through nine samplings of the longitudinal shower profile.

The characteristic signature of an electron is the development of an electromagnetic cascade which starts within the first radiation length of the shower detector and reaches maximum intensity at a depth varying from $\sim$5–10 radiation lengths over the energy range 5–500 GeV. Most of the electron energy is absorbed in the shower counter. Since the thickness

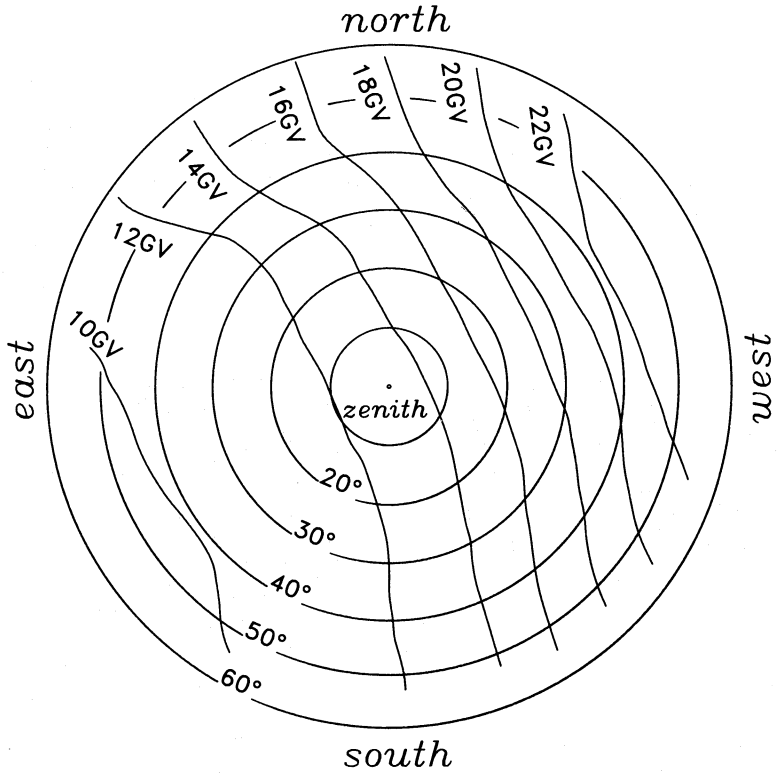

FIG. 2.—Contours of cutoff rigidities at Hawaii for negatrons

of the shower counter S corresponds to only 0.69 proton interaction lengths, protons will in general lead to distinctly different signals: they will either traverse the shower counter without interaction, or produce nuclear cascades with starting points almost equally distributed through the shower counter, and with a significant fraction of the proton energy escaping at the bottom. Approximately 1% of all protons may, however, interact within the first radiation length, producing one or more neutral pions which give rise to electromagnetic cascades that are indistinguishable from true electron showers. Since we require an overall rejection efficiency against protons of the order of 10^{-4}, we must utilize the TRD to remove this remaining proton background.

The TRD is designed such that only particles with Lorentz factors $\gamma = E/mc^2$ larger than 2×10^3 produce a measurable transition radiation (TR) signal, which approaches saturation (i.e., becomes independent of γ) for $\gamma > 10^4$. Thus, all electrons above ~ 5 GeV produce saturated TR signals, while protons cannot generate TR at all up to energies of a few TeV. The radiation is emitted with X-ray energies around 10 keV. We therefore use xenon-filled MWPCs as detectors. The TR signal is relatively weak, and is superposed upon the ionization signal of the parent particle. In order to optimize the electron-proton discrimination efficiency, we use a TRD consisting of a sandwich of six detectors, and we analyze the MWPC signals with a maximum likelihood technique. The overall acceptance efficiency of the TRD for electrons is 85% at a discrimination efficiency against protons of 3×10^{-2}. We note that the acceptance/rejection efficiency in the present flight is slightly worse than in our previous experiments. This is due to a somewhat degraded resolution of the MWPCs, caused by inferior purity of xenon available to us for this flight. However, the efficiency margin was sufficient for a safe identification of positrons.

The properties of this detector system have been quantitatively determined in extensive calibration measurements at accelerators (Müller 1972; Cherry *et al.* 1974; Prince 1979). Overall, the essential parameters at 10 GeV are the following:

Energy resolution for electron showers (1 σ) $\delta E/E = 8\%$;
Acceptance efficiency for electrons, 70%;
Rejection efficiency against protons, 3×10^{-4}.

During the balloon flight from Hawaii, the instrument has been suspended with its axis inclined by 30° against the vertical. The orientation of the gondola was measured with a two-axis fluxgate magnetometer. Through the use of a commandable torque motor, the instrument was oriented toward the west for the major part of the flight to observe positrons, or toward the east for a control measurement of negatrons.

III. DATA ANALYSIS AND RESULTS

a) Overview

The flight data are transmitted via telemetry and recorded on ground. A major part of the data analysis consists of selecting electrons within a large flux of mostly proton-induced background events. A discussion of the selection procedure will be given in § III*b*.

Once the electron fraction has been identified, we shall describe in § III*c* the grouping of electrons into energy intervals and according to their arrival directions. We shall define two energy spectra labeled "East" and "West." Each spectrum is a composite of galactic negatrons, galactic positrons, and secondary electrons which are either directly produced in the

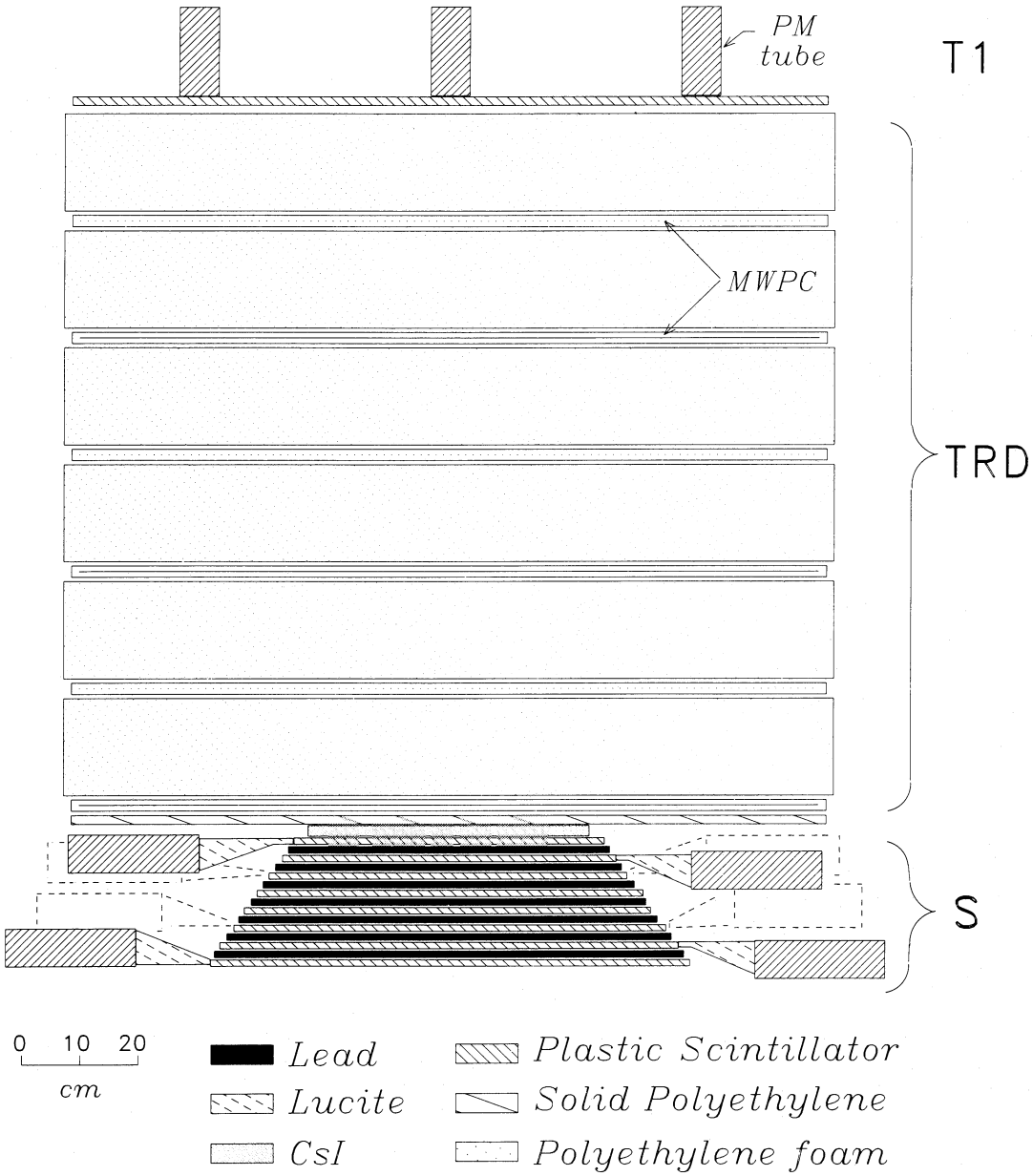

FIG. 3.—Schematic cross section of the instrument

atmosphere or which appear as reentrant albedo particles. Although these different types of electrons cannot be separated by the detector, they manifest themselves as distinct features in the composite energy spectra resulting from the geomagnetic cutoff effects. These features and the east/west asymmetry will be evident when the East and West spectra are compared with each other and with the electron spectrum measured previously at higher geomagnetic latitude (Tang 1984).

In § III*d* the positron fraction will be derived. The derivation is based on direct interpretation of the experimental data and does not require any detailed assumptions about the magnitude and shape of the various components of the measured spectra.

In § III*e* we present a more detailed analysis of the East and West spectra in terms of their various components: e^-, e^+, direct atmospheric secondary electrons, and reentrant albedo electrons. We shall show that the interpretation of our data is consistent with existing measurements and calculations concerning atmospheric secondaries and reentrant albedo electrons.

In § III*f*, we examine the background of interacting protons. We shall argue that this background does not significantly affect our results and conclusions.

b) Electron Selection

During the balloon flight, we record all particles which interact in the shower detector, thus excluding the large flux of protons which traverse without interaction. Nevertheless, the recorded data set is dominated by events due to interacting protons. The procedures employed to select electrons from these data are similar to the ones used in our previous experiment (Tang 1984).

First, events with an electric charge $Z > 1$ are rejected by requiring a signal in T1 due to a singly charged particle. Then the time-of-flight information and the multiwire chamber signals are used to select events with well-defined, downward-moving trajectories. Thus all upward-moving particles generated from interactions below the detector, and events which form multiple tracks in the TRD, are rejected. After these cuts, background proton events are still considerably more abundant than electron events.

The proton background is suppressed by a cut based on a least χ^2 analysis of the shower profile: for each event, the pulse heights from the nine scintillators of the shower detector S are compared with predicted profiles of electromagnetic showers (Müller 1972; Prince 1976) to obtain the electron energy E and the χ^2 parameter, which measures the deviation of the measured pulse heights from the best-fit predicted shower profile. While all electron events have χ^2 close to 1, most of the interacting protons are characterized by larger values of χ^2. After cutting events with $\chi^2 > 1$, $\sim 1\%$ of all cosmic-ray protons are still in the data set, indistinguishable from electrons.

The TRD is used to remove the remaining background. The TRD exhibits distinctly different signal distributions for electrons and protons: electrons are accompanied by transition radiation X-rays, while protons produce ionization signals only. The measured signals are analyzed by a maximum likelihood method (for details, see Cherry, Müller, and Prince 1974; Cherry *et al.* 1974). For every event a set of six signals x_i ($i = 1, \ldots, 6$) are measured along its trajectory in the six proportional chambers, and the likelihood parameter L is defined as

$$L = \prod_{i=1}^{6} [P_e^i(x_i)/P_p^i(x_i)] ,$$

where $P_e^i(x_i)$ is the probability that an electron generates pulse height x_i in the ith chamber ($i = 1, \ldots, 6$), and $P_p^i(x_i)$ is the probability that a proton generates pulse height x_i. Electrons are characterized by a L distribution which peaks at $L > 1$, while the proton distribution shows a well-separated peak at $L < 1$. Figure 4 shows a L distribution for this experiment. The events shown entered the detector from the west and have passed the criteria of clean tracks and $\chi^2 < 1$. The dashed curves indicate the expected distributions due to protons ($L < 1$) and electrons ($L > 1$). Rejecting events with $L < 1$ provides an additional discrimination against protons with an efficiency of 3×10^{-2}, while retaining $\sim 85\%$ of the electrons. Thus after this final data cut, a clean sample of electron events with a potential proton background well below 10% is obtained.

c) *Energy Spectra of Electrons*

The energy of every electron event is obtained from the shower detector. We emphasize that the absolute energy cali-

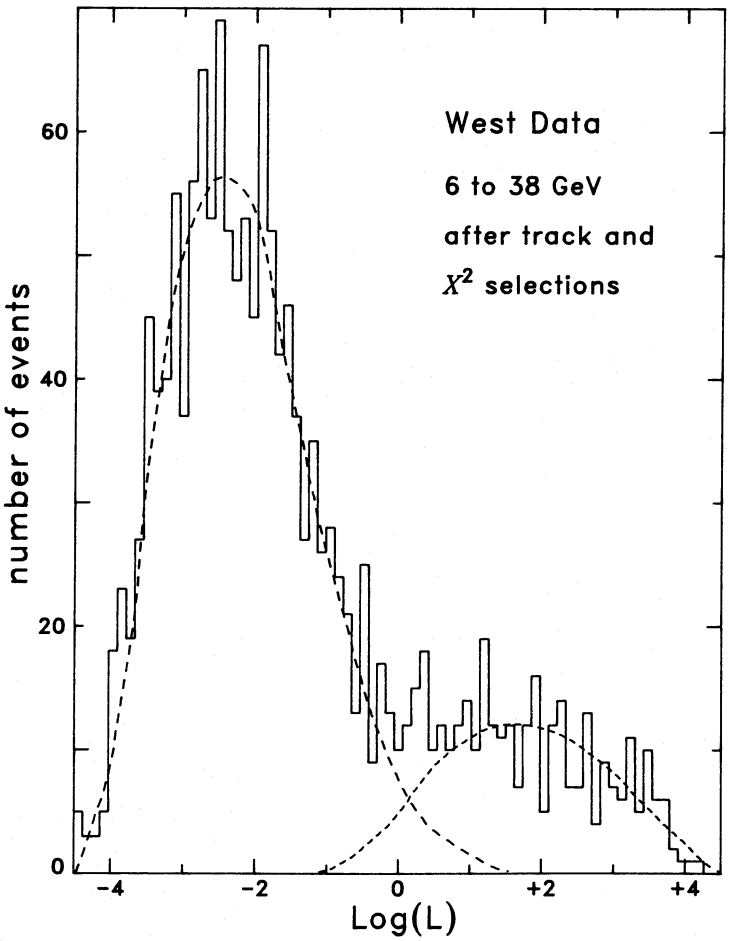

FIG. 4.—Likelihood distribution of flight data of this experiment

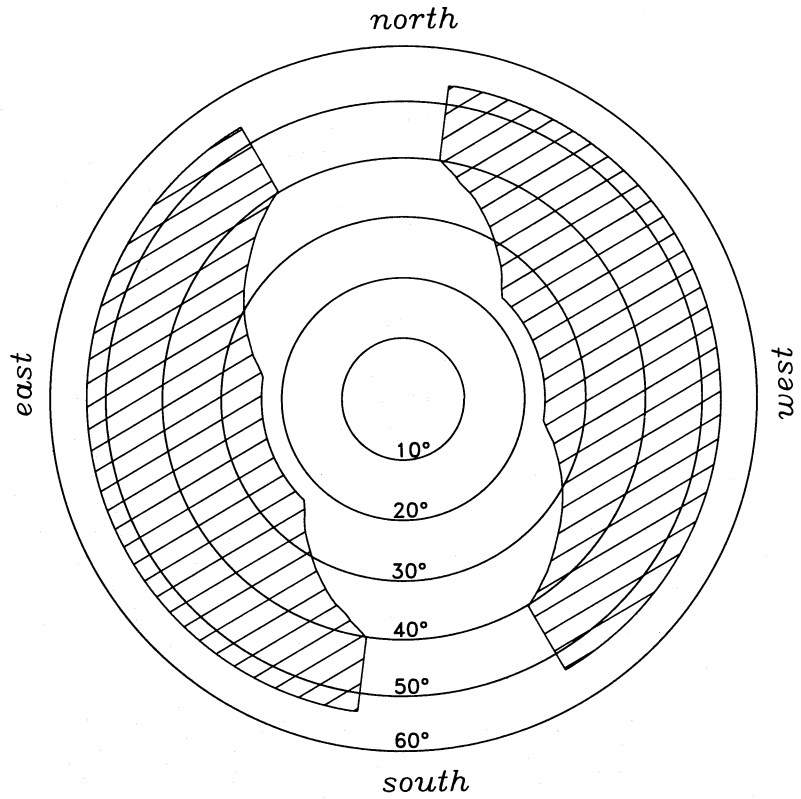

FIG. 5.—East and west incidence directions chosen for the analysis. Events within the shaded regions are analyzed to form the east and west energy spectra.

bration has been determined in accelerator tests (Müller 1972; Prince 1976). We apply a +5% correction to the measured energy in order to compensate for energy loss due to bremsstrahlung in the overlaying atmosphere. The events are grouped into various energy intervals and also into two main groups, East and West, according to their direction of incidence upon the detector. The zenith and azimuthal angles are derived from hodoscopic and magnetometer data with a resolution of $\delta\theta \approx 2°$. The shaded regions in Figure 5 correspond to portions of the sky accepted for these two groups. They are chosen on the basis of the cutoff rigidities (Fig. 2), which are determined using computer codes of Shea and Smart (1974). We note that the measurements of Jordan and Meyer (1983) have been in agreement with these predictions. The negatron cutoff is between 10 to 12 GV in the East region, and between 18 and 24 GV in the West region. For positrons, these two regions exchange roles. Events from other parts of the sky are not used in this analysis.

Table 1 outlines the derivation of the differential energy spectra of electrons incident from East and West. The numbers of events accepted as electrons are tabulated as N(total). The estimated numbers of residual background (mostly protons) within the accepted sample are listed as N(proton). The overall efficiency factors f for electron acceptance are also tabulated. These factors are obtained from our previous work with this instrument (Tang 1984) and are based on calibration data obtained at accelerators. They take into account efficiencies in the selection of singly charged particles, in the determination of

TABLE 1

SUMMARY OF ELECTRON FLUX MEASUREMENT

ENERGY (GeV)	f	WEST			EAST		
		N(total)	N(proton)	dN_e/dE	N(total)	N(proton)	dN_e/dE
4.8– 5.6.....	0.70	64	2.6	0.208 ± 0.027	21	0.25	0.196 ± 0.044
5.6– 6.6.....	0.70	56	3.9	0.141 ± 0.020	15	0.25	0.111 ± 0.030
6.6– 8.0.....	0.70	44	4.8	0.076 ± 0.013	22	0.45	0.116 ± 0.026
8.0–10.0.....	0.68	34	7.1	0.037 ± 0.009	10	0.55	0.037 ± 0.013
10.0–12.2.....	0.66	40	5.8	0.045 ± 0.009	22	0.60	0.078 ± 0.017
12.2–14.4.....	0.62	27	3.5	0.033 ± 0.007	25	0.55	0.095 ± 0.019
14.4–17.0.....	0.60	21	2.0	0.023 ± 0.006	23	0.90	0.075 ± 0.017
17.0–20.0.....	0.56	13	1.3	0.013 ± 0.004	17	0.45	0.052 ± 0.013
20.0–24.0.....	0.52	20	0.8	0.017 ± 0.004	10	0.25	0.025 ± 0.008
24.0–28.0.....	0.50	18	0.3	0.017 ± 0.004	9	0.10	0.024 ± 0.008
28.0–32.0.....	0.48	12	0.3	0.012 ± 0.003	2	0.10	0.005 ± 0.004
32.0–38.0.....	0.45	10	0.4	0.007 ± 0.003	2	0.00	0.004 ± 0.003

the trajectories through the instrument, and in the cuts on the parameter χ^2. The major contributor of inefficiency is the track selection procedure. We note that the efficiency factors have a smooth, monotonic energy dependence, which implies that the various features in the energy spectra which we are about to report cannot be due to sudden changes in acceptance efficiencies. The exposure factors G are 528 m^2 sr s and 189 m^2 sr s, respectively, for the data obtained from West and East. Their ratio, G(west)/G(east), is determined with an accuracy of about $\pm 5\%$. The absolute normalization of G, however, has a larger uncertainty of $\pm 10\%$. The differential energy spectrum is then obtained by

$$\frac{dN_e}{dE} = \frac{N(\text{total}) - N(\text{proton})}{\Delta E f G},$$

The resulting energy spectra for both East and West are shown in Figure 6. They are the spectra for all electrons observed by the detector. In Figure 6, the horizontal error bars represent the bin sizes, and the vertical bars include both statistical and systematic errors. The dashed and solid curves are hand fits to the East and West data, respectively, to facilitate a ready comparison of the two spectra. The shaded region represents, also for the purpose of comparison, the primary electron spectrum undisturbed by geomagnetic effects. That spectrum was reported previously (Tang 1984) on the basis of balloon flights at lower geomagnetic cutoff locations. For the rest of this paper, we shall refer to this spectrum as N_e^{tot}.

At high energies (>25 GeV), both East and West spectra agree with N_e^{tot}, but at lower energies significant cutoffs are apparent. Particles arriving from the East show a sharp cutoff feature at ~11 GeV, while the flux of particles arriving from the west appears to be suppressed by geomagnetic effects up to

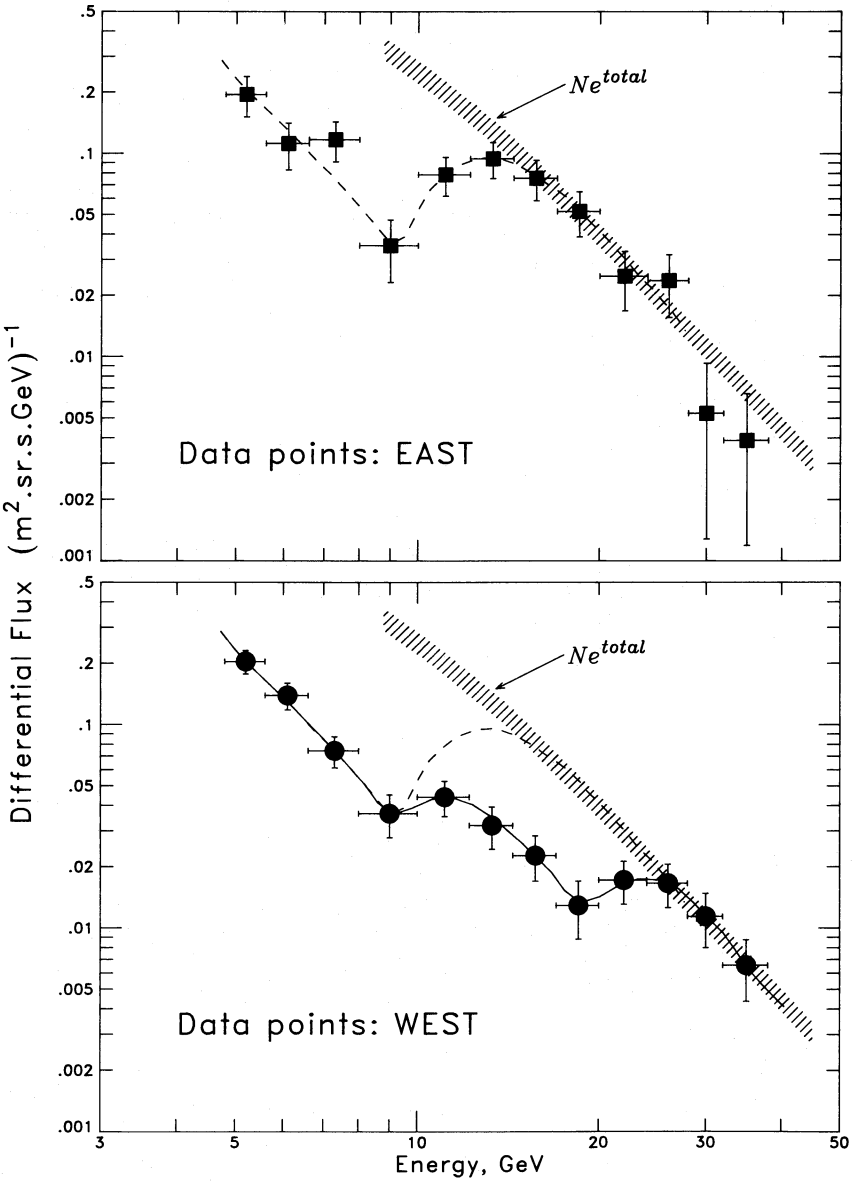

FIG. 6.—East and west energy spectra measured in this experiment. Shaded region N_e^{tot} is the electron spectrum measured at a low geomagnetic cutoff region (Tang 1984).

energies around 25 GeV. A pronounced east-west asymmetry can be seen in the energy region from 10 to 20 GeV where the geomagnetic field forbids negatrons from arriving from the west but not from the east. This asymmetry implies that cosmic-ray negatrons are more abundant than positrons at these energies.

Below 10 GeV, one expects primary cosmic-ray electrons to be cut off from all incidence directions by the geomagnetic field. Particles observed in this energy region must be of atmospheric secondary origin, either produced directly in the overlaying atmosphere, or appearing as return-albedo electrons. Since the parent protons have on the average more than 5 times the energy of the secondary electrons (Orth and Buffington 1976), the flux of secondaries from 5 to 10 GeV is expected not to be affected by the geomagnetic cutoff and hence to show no east/west asymmetry. This is in very good agreement with the measured spectra shown in Figure 6.

d) Derivation of the Positron Fraction

The effect of the geomagnetic cutoff on the East and West spectra, as described in the previous section, has the following implications: (i) the electron flux below 10 GeV is a measure of the background caused by electrons of secondary origin, (ii) below 20 GeV in the West spectrum, all primary negatrons are forbidden, and the observed flux is a sum of primary positrons and background. These observations alone allow the positron fraction $e^+/(e^+ + e^-)$ to be derived in the region of 10–20 GeV without requiring detailed assumptions.

The background spectrum from 5 to 10 GeV can be fitted very well to a power-law form, which can be extrapolated to higher energies as shown by the dotted area in Figure 7. We conservatively assign a large uncertainty to this extrapolation. Even with this sizable uncertainty, there is an unambiguous enhancement of flux above the background from 10 to 20 GeV. We identify this excess as the positron signal.

The shaded region in Figure 7 represents the spectrum of the sum of primary negatrons and positrons undisturbed by the geomagnetic field. This is the N_e^{tot} spectrum shown also in Figure 6. The width of the shaded region represents the estimated errors, including uncertainties in the exposure factors of the measurements.

To summarize, in the region of 10–20 GeV, we have determined the following quantities: (i) the sum of positrons and background secondary electrons, (ii) the extrapolation of the background from lower energies, and (iii) the sum of all electrons. These quantities are tabulated with error estimates in Table 2 as N(pos + atmos), N(atmos), N(sum) respectively. The data in Table 2 are divided into just two bins for better counting statistics, and the fluxes are presented as numbers of events to emphasize the role of statistics. By presenting the result as the positron fraction $e^+/(e^+ + e^-)$ and not the absolute positron flux, one avoids uncertainties due to errors in the exposure factor and acceptance efficiencies.

We have also considered the smearing of the sharp cutoff features, which is caused by limited energy resolution (8% standard deviation) of the detector and by errors in computing the directions of incidence of the particles. Another contribution comes from the stochastic loss of energy in the overlaying atmosphere. As a consequence, the number of positrons near and above the positron cutoff will be underestimated because of positrons spilling over to a lower energy interval. On the other hand, just below the negatron cutoff, the number of positrons will be overestimated because of some spilling over of negatrons from above. We have estimated these effects by numerical calculations. Adjustments ($\pm 5\%$) on the positron counts are made by introducing a multiplicative factor h in Table 2.

Finally, as listed in Table 2, with $N(\text{pos}) = N(\text{pos} + \text{atmos}) - N(\text{atmos})$, the positron fraction of cosmic-ray electrons is given by

$$\frac{e^+}{(e^+ + e^-)} = \frac{N(\text{pos})h}{[N(\text{sum}) - N(\text{atmos})]} .$$

e) Comparison with Numerical Predictions

We have assumed that the measured flux below 10 GeV is dominated by secondary electrons and that the West flux between 10 and 20 GeV consists of only positrons superposed

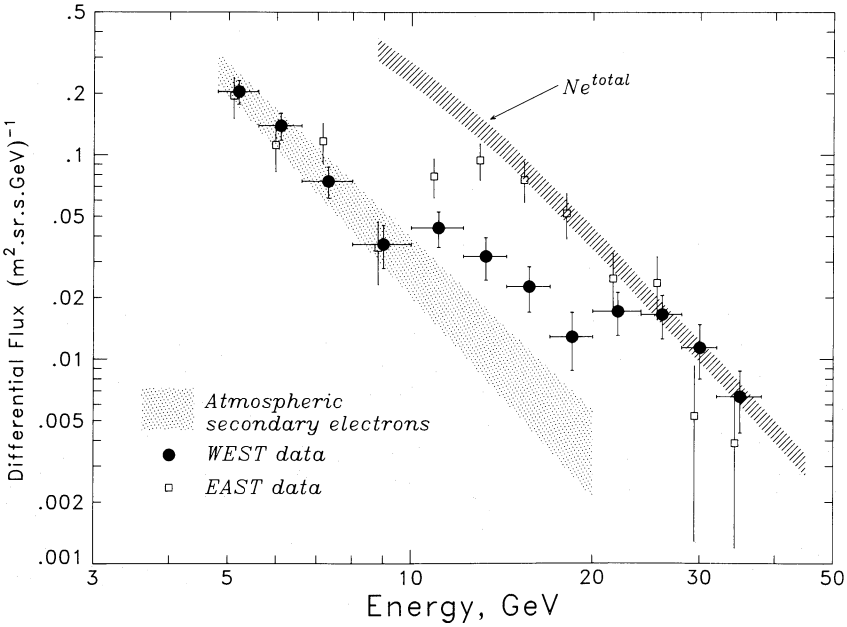

FIG. 7.—Extrapolation for estimating the background of atmospheric secondary electrons. N_e^{tot} is the same as in Fig. 6.

TABLE 2

SUMMARY OF POSITRON FRACTION COMPUTATION

E(GeV)	N(pos + atmos)	N(atmos)	N(sum)	N(pos)	h	$e^+/(e^+ + e^-)$
10.0–14.4.....	57.7 ± 8.5	22.0 ± 5.8	270 ± 29	35.7 ± 10.0	1.05 ± 0.05	0.151 ± 0.048
14.4–20.0.....	30.7 ± 5.9	8.6 ± 3.4	106 ± 13	22.1 ± 7.0	0.90 ± 0.10	0.204 ± 0.072

on the background. This picture is based on the fact that galactic negatrons are cut off below 20 GeV in the West spectrum and positrons are cut off below 10 GeV. We shall now show that this analysis is in good agreement with existing measurements and predictions concerning the geomagnetic cutoff, the overall galactic electron spectrum, and the atmospheric secondary electron flux.

We fit the measured East and West spectra each as a superposition of four components: direct atmospheric secondary electrons (S1), reentrant albedo electrons (S2), galactic negatrons (e^-), and galactic positrons (e^+). S1 and S2 together form the background of secondary particles discussed in the previous section.

We estimate the flux of secondary electrons generated by cosmic rays directly above the instrument on the basis of the calculation by Beuermann (1971). The curve (S1) in Figure 8, which is the same for East and West, shows the predicted flux of secondary electrons for 7 g cm^{-2} of air, which is the average amount of residual atmosphere for this experiment, taking the distribution of zenith angles into account.

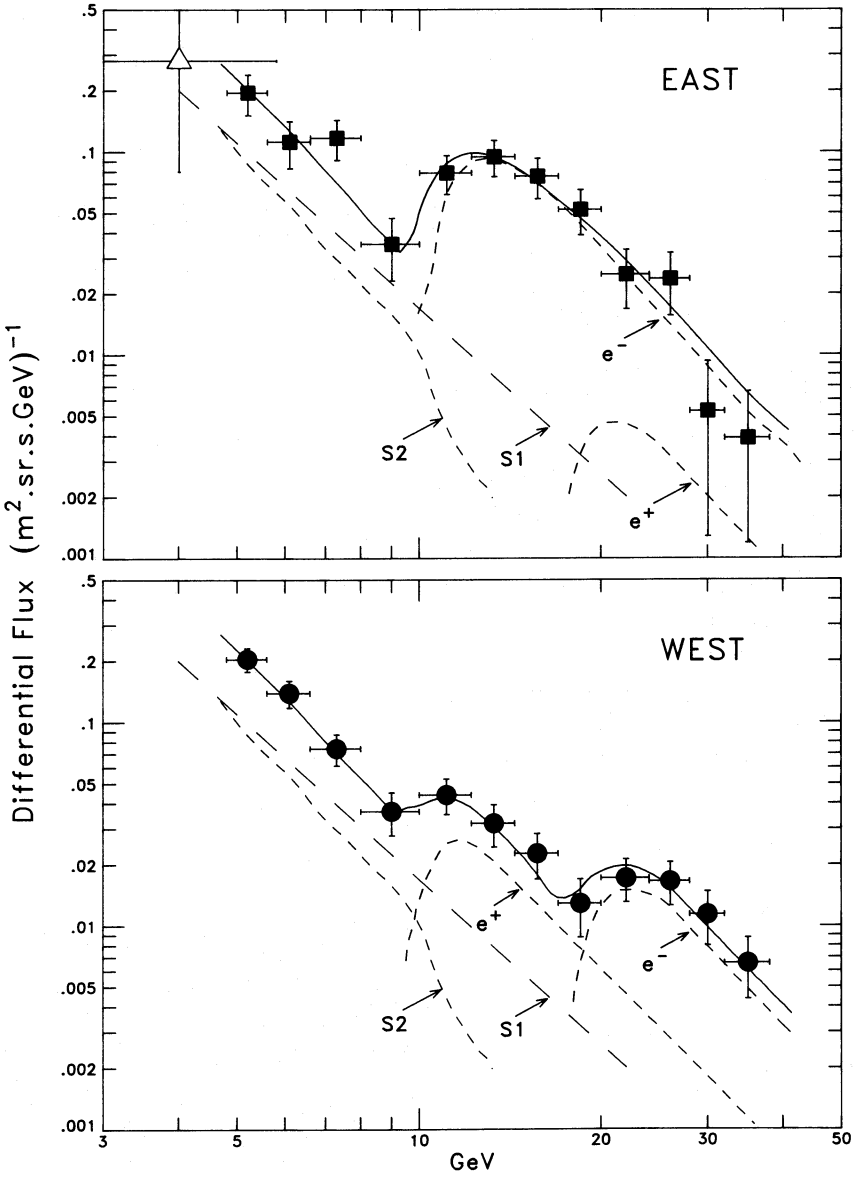

FIG. 8.—Fitting the spectra with four components: galactic negatrons (e^-), galactic positrons (e^+), direct atmospheric secondary electrons (S1), and reentrant albedo electrons (S2). Open triangle shows the flux of reentrant albedo electrons measured by Daniel and Stephens (1967).

This predicted contribution from direct atmospheric secondary electrons (S1) is significantly lower than the measured flux between 5 and 10 GeV. Since all primary electrons are forbidden in this energy region, we attribute the excess flux to reentrant albedo electrons, i.e., up-splash atmospheric secondaries that are bent back to Earth by the geomagnetic field. The curve (S2) in Figure 8 is the needed contribution from albedo atmospheric secondaries such that the sum of curves (S1) and (S2) accounts for the measured flux below 10 GeV. Very little experimental information on reentrant albedo electrons above a few GeV is available to test this assumption. We include in Figure 8 one such measurement at 4 GeV (Daniel and Stephens 1965). This datum is consistent with our prediction. The reentrant flux (S2) that best fits our data exhibits a slightly steeper spectrum than S1, but this difference in slope is not significant within the uncertainties of the measurement. At energies above the geomagnetic cutoff, the reentrant particle flux is expected to diminish further because the up-splash secondaries can then escape from Earth.

The flux increase above 10 GeV must be due to galactic positrons (e^+) and negatrons (e^-). We know the overall electron spectrum in the absence of the geomagnetic effect, namely, spectrum $N_e^{\rm tot}$ of Figure 6. A positron fraction $e^+/(e^+ + e^-)$ of 20% provides an approximate fit to the data in the following way: we fold the e^+ and e^- spectra (in the proportions 20% and 80%, but assuming the same spectral slope) with the geomagnetic cutoff structure at Hawaii as given by the computer codes of Shea and Smart (1974). We also include in this calculation the distribution of particle incidence directions and the energy resolution of the detector. This leads to curves "e^-" and "e^+" for each incidence direction in Figure 8.

The solid curves in Figure 8 are the sum of e^-, e^+, S1, and S2. They fit the data points for both the East and West spectra, demonstrating that the limited energy resolution of the detector and the variation of the cutoff rigidities do not severely broaden the cutoff features. In summary, our measurements and interpretation are consistent with the predictions available with respect to the atmospheric and reentrant albedo background, and to the characteristic energies and sharpness of the geomagnetic cutoffs.

f) *Interacting Protons*

Protons have the same geomagnetic cutoff rigidity as positrons. It is therefore very important to make sure that the flux enhancement which we claim to be positrons is not contaminated by residual events generated by protons. We shall demonstrate that this is indeed not the case.

The proton rejection power of this instrument, with its transition radiation detector and shower counter, has been proven to be $\sim 10^4$ in accelerator calibrations and cosmic-ray measurements (Prince 1976; Tang 1984). The proton/electron separation for this experiment is illustrated in the likelihood (L) distributions in Figure 4. This proton/electron separation, although not quite as good as in our previous measurement (Tang 1984), is adequate to reduce the final required subtraction of background events to a few percent of all accepted electrons (see Table 1).

We can also examine the effect of interacting protons on the energy spectrum. The energy measured in this experiment is actually the energy deposited by the cascade of interactions at the shower counter. If the cascade is generated by an electron, almost the entire energy of the primary electron is absorbed. However, if the electromagnetic cascade is generated by neutral pions produced in a nuclear interaction, a substantial fraction of the primary energy may be retained in hadrons. The apparent energy measured is, in general, smaller than the true proton energy, and the ratio of apparent energy to true energy has a broad distribution. This fact can be demonstrated with data from this experiment. The distribution of the measured energy for interacting protons from the west is shown in Figure 9. The protons in this sample show no transition radiation ($L < 1$), but their shower profiles are indistinguishable from those of the electrons ($\chi^2 < 1$). The true energies of these protons have a cutoff at 10–11 GeV, but their energies deposited at the shower counter show a distribution peaked around 7 GeV. Figure 9 also shows the distribution of electrons from the west. We recall (see, e.g., Fig. 8) that the enhanced electron flux at 10–20 GeV above the level of atmospheric secondary electrons is interpreted as the positron signal. Because of their very different energy distributions, interacting protons cannot be the cause for this feature in the electron spectrum.

IV. DISCUSSION

The positron fraction of cosmic-ray electrons, $e^+/(e^+ + e^-)$, obtained in this experiment from 10 to 20 GeV is listed in Table 2. The error limits include statistical as well as systematic uncertainties. This result is also shown in Figure 10, together with results from other positron measurements.

Our result, while consistent with the limit set by Buffington, Orth, and Smoot (1975), is significantly higher than the positron fraction measured from 1 to 10 GeV. This increase has not been predicted by calculations of cosmic-ray propagation (Ramaty 1974; Orth and Buffington 1976; Protheroe 1982).

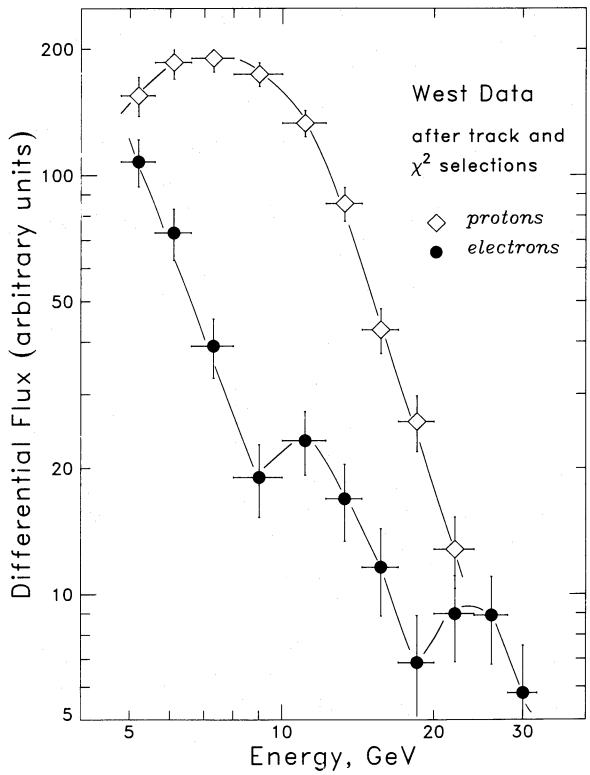

FIG. 9.—Comparison of the energy distribution of electrons with that of protons which interact in the shower detector to form cascades indistinguishable from true electron showers.

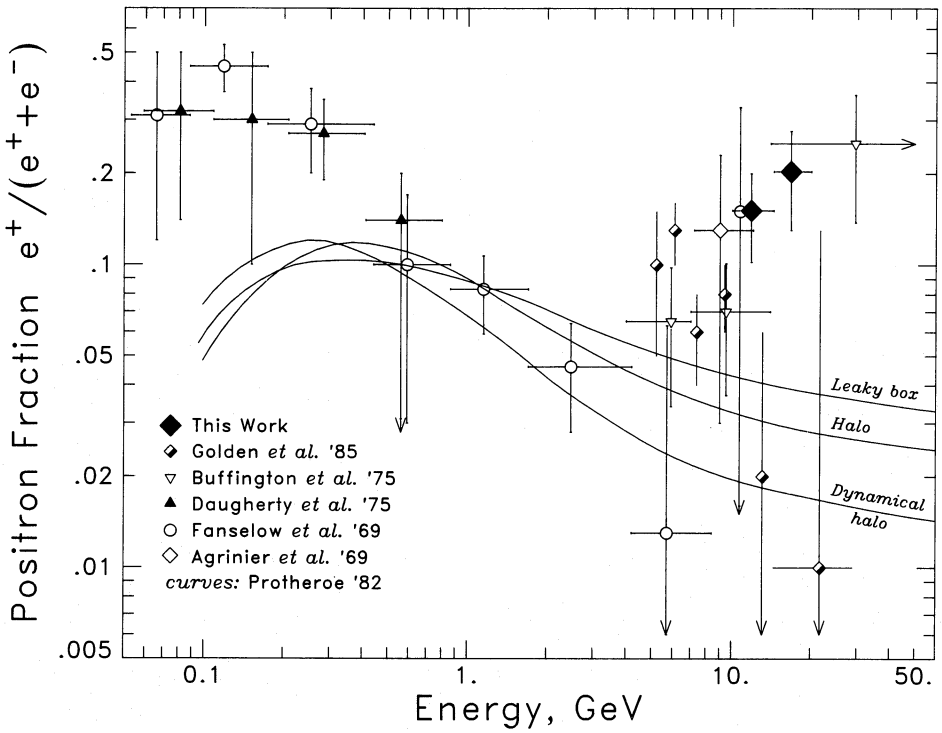

FIG. 10.—Positron fraction of cosmic-ray electrons

Using an interstellar path length of ~ 4 g cm^{-2}, which is consistent with data on nuclear spallation, these calculations fit the positron fraction reported between 1 and 10 GeV quite well. As an example, Figure 10 shows the calculations by Protheroe (1982) for three different propagation models. The calculation also indicated that the positrons from 1 to 10 GeV are essentially secondary particles produced by cosmic rays (mostly protons) in the interstellar medium. Protheroe (1982) estimated that at most 3% of the observed positrons can be of primary origin. Our results at higher energy would fit this model only if the path length were increased to ~ 15 g cm^{-2}. This however, would be inconsistent with the low-energy data.

There are two possible ways to understand this behavior of the positron/electron ratio: (1) the primary component of positrons, although insignificant below 10 GeV, increases substantially above 10 GeV, or (2) the spectrum of primary electrons (almost entirely negatrons) decreases above 10 GeV more sharply than that of secondary positrons. There is no independent information at present that would support the first possibility. The second case, however, warrants some further comment.

We note that the positron fraction shown in Figure 10 appears to increase at just the same energy ($\gtrsim 10$ GeV) where the overall electron spectrum (Fig. 1) starts to become steeper than that of protons. This may suggest that the spectrum of positrons does not experience a steepening at 10 GeV but continues with the same slope as that of the parent protons to higher energies. The depletion of the primary negatrons above 10 GeV may be caused by a cutoff at the acceleration site (perhaps due to synchrotron losses in a relatively strong magnetic field at the source location), or it could be the consequence of a large spatial distance between the electron source and the solar system. These suggestions, which are highly speculative at present, predict that the positron fraction will increase to $\sim 50\%$ at higher energies. It is obvious that further measurements of positrons, extending to higher energies, must solve this question.

We wish to thank Mr. Eugene Drag for the electronics work and help during the balloon flight expedition and Dr. Richard Kroeger for many contributions in the conduct of this experiment. We sincerely thank the team of Professor Peter Meyer, Dr. Steve Jordan, and Mr. John Grunsfeld for generously sharing their equipment and facilities with us. The excellent service and support of the National Scientific Balloon Facility and of the US Navy are deeply appreciated. In particular, we acknowledge the efforts of Mr. Robert Kubara of the NSBF and of Mr. Stewart Burley of the US Navy Pacific Missile Range Facility.

REFERENCES

Agrinier, B., *et al.* 1969, *Lett. Nuovo Cimento*, ser. 1, **1**, 53.
Anand, K. C., Daniel, R. R., and Stephens, S. A. 1969, *Proc. 11th Internat. Cosmic-Ray Conf.* (Budapest), **1**, 235.
Beuerman, K. P. 1971, *J. Geophys. Res.*, **76**, 4291.
Beuerman, K. P., Rice, C. J., Stone, E. C., and Vogt, R. E. 1970, *Acta Phys. Acad. Sci. Hungaricae*, Vol. **29**, Suppl. No. 1, p. 173.
Buffington, A., Orth, C. D., and Smoot, G. F. 1975, *Ap. J.*, **199**, 699.
Cherry, M. L., Hartmann, G., Müller, D., and Prince, T. A. 1974, *Phys. Rev. D*, **10**, 3594.
Cherry, M. L., Müller, D., and Prince, T. A. 1974, *Nucl. Instr. Methods*, **115**, 141.
Daniel, R. R., and Stephens, S. A. 1965, *Phys. Rev. Letters*, **15**, 769.
———. 1967, *Proc. Indian Acad. Sci.*, **65a**, 319.
Daugherty, J. K., Hartman, R. C., and Schmidt, P. J. 1975, *Ap. J.*, **198**, 493.

Fanselow, J. L., Hartman, R. C., Hildebrand, R. H., and Meyer, P. 1969, *Ap. J.*, **158**, 771.
Garcia-Munoz, M., Mason, G. M., and Simpson, J. A. 1977, *Ap. J.*, **217**, 859.
Golden, R. L., Mauger, S., Badhwar, G. D., Daniel, R. R., Lacy, J. L., Stephens, S. A., and Zipse, J. E. 1984, *Ap. J.*, **287**, 622.
Golden, R. L., *et al.* 1985, *Proc. 19th Internat. Cosmic-Ray Conf.* (La Jolla), **OG 2**, 374.
Hartmann, G., Müller, D., and Prince, T. A. 1977, *Proc. 15th Internat. Cosmic-Ray Conf.* (Plovidiv), **1**, 366.
Jordan, S., and Meyer, P. 1983, *Proc. 18th Internat. Cosmic-Ray Conf.*, **OG**, 45.
Juliusson, E., Meyer, P., and Müller, D. 1972, *Phys. Rev. Letters*, **29**, 445.
Müller, D. 1972, *Phys. Rev. D*, **5**, 2677.
Nishimura, J., *et al.* 1981, *Proc. 17th Internat. Cosmic-Ray Conf.* (Paris), **2**, 94 (Japan-US Primary Electron Collaboration).
Orth, C. D., and Buffington, A. 1976, *Ap. J.*, **206**, 312.
Prince, T. A. 1979, *Ap. J.*, **227**, 676.
Protheroe, R. J. 1982, *Ap. J.*, **254**, 391.
Ramaty, R. 1974, in *High Energy Particles and Quanta in Astrophysics*, ed. F. B. McDonald and C. E. Fichtel (Boston: MIT Press), pp. 122–169.
Shea, M. A., and Smart, D. F. 1974, Air Force Cambridge Research Lab., Tech. Rep. AFCRL-TR-74-0159.
Tang, K. 1984, *Ap. J.*, **278**, 881.
Wiedenbeck, M. E., and Greiner, D. E. 1980, *Ap. J.* (*Letters*), **239**, L139.

D. MÜLLER and K. TANG: Enrico Fermi Institute, University of Chicago, 933 E. 56th St., Chicago, IL 60637